



Rice-Like ZnO Architecture: An Eminent Electrode Material for High-Performance Ultracapacitor Application

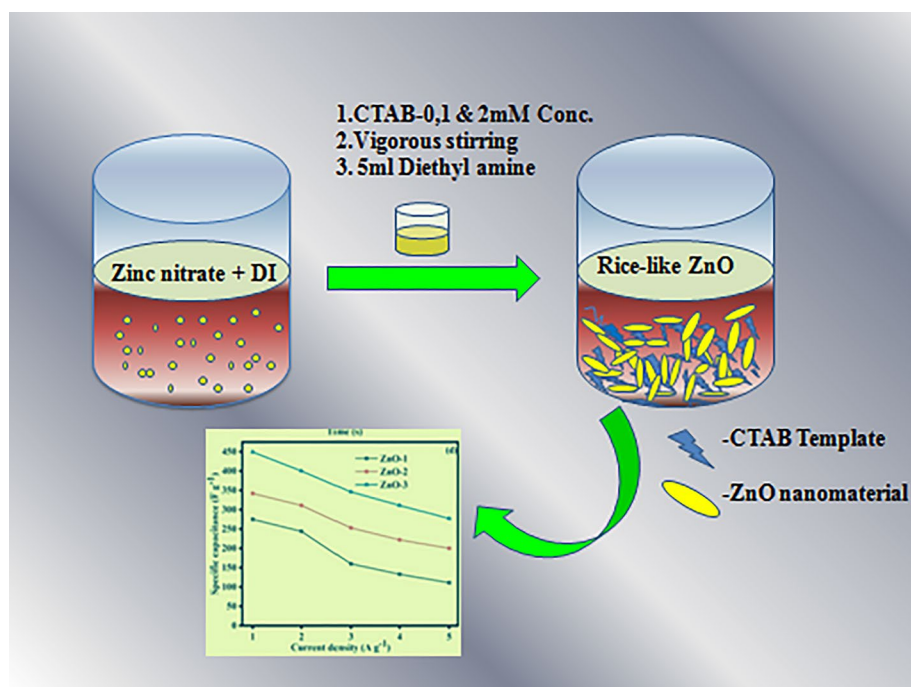
Kunhikrishnan Lakshmi^{1,2} · Shanmugham Revathi¹

Received: 29 September 2020 / Accepted: 27 January 2021 / Published online: 20 February 2021
© The Author(s), under exclusive licence to Springer Science+Business Media, LLC part of Springer Nature 2021

Abstract

In this investigation, the rice-like ZnO material was successfully synthesized using the CTAB assisted chemical co-precipitation method followed by a probable annealing process. The internal structure, thermal properties, phase studies, and morphological features were analyzed using Fourier transform infrared spectroscopy (FTIR), Thermogravimetric analysis (TGA), X-ray diffraction analysis (XRD), and scanning electron microscopy (SEM) techniques, respectively. The CTAB serves as a template that influences the fabrication process and exclusively alters ZnO materials' morphological features. The high concentration of the CTAB (2 mM) template provides a rice-like ZnO structure. The synthesized ZnO material's electrochemical properties were inspected using cyclic voltammetry (CV) and galvanostatic charge/discharge studies (GCD). The CV curves provide a specific capacitance of 457 F g^{-1} at a scan rate of 5 mVs^{-1} , whereas the GCD curves affirm a specific capacitance of 449 F g^{-1} at a current density of 1 Ag^{-1} . Furthermore, it also exhibits high cyclic stability with 94% of the initial capacitance retained even after continuous 2000 CV cycles at a scan rate of 100 mV s^{-1} . These results signify that the rice-like ZnO material could be a significant postulant for ultra-capacitor electrode applications.

Graphic Abstract



Keywords Rice-like structure · ZnO · CTAB · Co-precipitation · Energy storage · Ultracapacitors

Extended author information available on the last page of the article

1 Introduction

The controllable preparation of various dimensional nanostructured materials has attracted significant attention from theoretical and commercial perspectives since they possess different optical and electrical properties [1, 2]. Of late zinc oxide (ZnO) based nanostructured materials have established significant concern due to their multifaceted applications in different fields. It also exhibits attractive optical and electronic properties. ZnO is a semiconductor material obtained from the II–VI group, which exhibits a high excitation binding energy of 60 meV, a bandgap of 3.37 eV, and good thermal stability [3, 4]. Additionally, ZnO possesses many benefits, including cost-effectiveness, eco-friendly, non-toxicity, and plentifulness. These excellent features of ZnO make it an exclusive material in electronic industries [5], photo catalysis [6], solar cells [7], gas sensing [8], drug carriers [9], biosensors [10], light-emitting diodes [11] and humidity sensors [12].

It is well known that varying preparation techniques and stoichiometric parameters can modify the nanoparticles' size, shape, and morphological features. Various synthetic routes such as chemical vapor deposition [13], hydrothermal method [14], solvothermal method [15], laser ablation [16], green synthesis using natural products [17], and electrochemical depositions [18] have been utilized to prepare nanostructured ZnO material. These synthetic routes have disadvantages such as the complex progression, high-cost precursor substance, and demands very rigorous control of different dispensation factors along with low productivity, high power utilization, and tedious manufacturing strategies, eco-unfriendly nature, and high production cost. Furthermore, it may be hard to be perceived at a large manufacturing scale. The facile and profitable method is necessary to prepare nanostructure materials to overcome these problems. Since Zinc oxide also exhibits morphologically dependent characteristics, selecting appropriate preparation routes, which influences appreciably deciding nanoparticles' characteristics, was focused.

Many synthetic methods have been established to prepare nanostructured ZnO material with suitable properties. Among the synthetic routes, simple chemical co-precipitation is an ideal method to prepare nanostructured materials owing to its low cost and simple equipment requirement [19]. On the other hand, disadvantage of this method is that the freshly prepared nanomaterials exhibit an agglomeration nature, restricting their performance in various application fields. Consequently, it is essential to prepare ZnO material with high dispersion ability to further enhance the performance through a co-precipitation synthetic route [20].

Adding a template is a practical approach to overcome the low dispersion and the restriction of aggregation

during nanoparticle formation. Templated precipitation is one of the most studied synthetic approaches for the generation of nanoparticles. Added templates that have some favored chemical entities bind the surface of nanoparticles; restricts their unrestricted formation, resulting in the particles' preferred size. The particle size of the nanomaterial is determined by the structure around the inorganic nano-sized center of surfactant molecules. The repulsive force restricts agglomeration between the nanoparticles between particles. These repulsions are due to electrostatic repulsion or steric exclusion between passivating agents. The nanoparticles' size and morphology are highly reliant on the surfactant used for the synthesis [21]. Till now, various types of templates such as polyvinyl alcohol (PVA) [22], CTAB [23], and bio-molecules [24] have been used to prepare nanostructured materials. Among them, CTAB is a template that can restrict the aggregation and facilitates the dispersion of nanoparticles. The template CTAB undertakes a vital responsibility in scheming the nucleation, altering morphological features, and developing the samples.

The cationic template CTAB will be separated as CTA^+ and Br^- ions respectively when it dissolves in solvents such as ethanol and water. Generally, the ZnO crystal exhibits a polar axis that exhibits positive and negative faces due to the unequal dispersal of Zn and O atoms. The Zn entity's positive face is placed by the Zn entity, whereas the O atoms occupy the negative face of the crystal. Consequently, the CTAB ions such as CTA^+ and Br^- alter the ZnO materials' surface morphological properties. Also, CTAB template form micelles or reverse micelles when it dissolves in solvents, which play a significant role in ZnO materials' morphology. The CTAB template acts as a growth controller and agglomeration inhibitor to obtain principle-oriented nanostructure [23]. Consequently, the CTAB templated co-precipitation method is an effective method to prepared nano sculptured ZnO material.

In this article, a rice-like ZnO structure was developed using CTAB assisted chemical co-precipitation method followed by a proper annealing process. The prepared ZnO materials were used as electrode materials for supercapacitor application. Two different CTAB template concentrations were utilized to access potential physicochemical differences in the final products. The physicochemical properties of freshly prepared ZnO material were analyzed using TGA, FTIR, XRD, and SEM techniques. It confirms the thermal behavior, crystalline phase, bonding nature, and morphological features of the ZnO material. The freshly prepared ZnO material's electrochemical features were analyzed using cyclic voltammetric and galvanostatic charge/discharge. The cyclic voltammetry curves provide the specific capacitance of 457 Fg^{-1} at a scan rate of 5 mVs^{-1} , whereas the galvanostatic charge/discharge curves display the specific

capacitance of 449 Fg^{-1} at a current density of 1 Ag^{-1} . The synthesis route and the supercapacitor study presented here is facile, cost-effective, robust, and eco-friendly.

2 Experimental Section

2.1 Materials

Every reagent used in this investigation is of analytical grade, without further purification. Carbon black, diethylamine ($(\text{CH}_3\text{CH}_2)_2\text{NH}$), Zinc nitrate hexahydrate ($\text{Zn}(\text{NO}_3)_2 \cdot 6\text{H}_2\text{O}$), poly(vinylidene fluoride) (PVDF), and Cetyltrimethylammonium bromide (CTAB) were obtained from Sigma Aldrich. Moreover, N-methyl-2-pyrrolidone (NMP) and nickel foil (0.025 mm thickness) were bought from Alfa aesar. In this study, de-ionized (DI) water was utilized as a solvent throughout the process.

2.2 Preparation of ZnO Materials

The ZnO materials were prepared through the CTAB assisted chemical co-precipitation technique. The synthetic process was carried out at room temperature. In a typical process, cationic surfactant CTAB was well dissolved in 100 mL DI water through continuous stirring until a homogeneous solution was obtained. Then, 0.1 M (2.9749 g) of Zinc nitrate hexahydrate was dissolved in a separate 100 mL beaker under continuous stirring. After that, the 100 mL aqueous Zinc nitrate solution was slowly added to the CTAB solution and was stirred vigorously for 1 h. When the mixed precursor solution became homogeneous, 5 mL of diethylamine was added dropwise to result in a white precipitate. The white precipitate was washed with ethanol and water multiple times to remove the impurities and CTAB template, and then was placed in the hot air oven for 24 h for drying. The resultant product was annealed at $600 \text{ }^\circ\text{C}$ for 4 h at a heating rate of $10 \text{ }^\circ\text{C min}^{-1}$ to acquire the final material. During the annealing process, the remaining impurities and templates were expelled entirely from the final product. The samples, namely ZnO-1, ZnO-2, and ZnO-3 were produced employing 0, 1, and 2 mM concentrations of CTAB.

2.3 Material Characterization of ZnO

The thermal properties of the ZnO material were characterized using NETZSCH STA 2500 TGA/DTA Instrument. The phase, purity, and crystalline behavior of ZnO material was evaluated using X-ray diffraction patterns (XRD) studies (PANalytical X-pert PRO diffractometer). Furthermore, ZnO materials' bonding properties were analyzed using Perkin-Elmer RX1' spectrophotometer with 4 cm^{-1} resolution applying compressed KBr pellets. The scanning

micron spectroscopic analyses were carried out in VEGA 3 TESCON and a Thermo scientific instrument (Quattro environmental scanning electron microscopy) instruments.

2.4 Electrode Preparation for Supercapacitor Analysis

The working electrodes for supercapacitor characterization were fabricated by the following method. The ZnO active material, poly (vinylidene difluoride) (PVDF) and acetylene black (80:10:10) were blended in an agate mortar with a few drops of 1-methyl-2-pyrrolidinone (NMP) solvent, and this mixture was made into a slurry. The resultant slurry was slowly coated on the nickel foil, and it was dried in a hot air oven at $70 \text{ }^\circ\text{C}$ for 6 h. The active material weight was approximately 3 mg. The electrochemical characteristics of freshly prepared ZnO material were demonstrated utilizing three electrodes set up in an aqueous 1 M KOH electrolyte. CHI 660B electrochemical workstation was used to analyze electrochemical properties in this demonstration. The ZnO coated nickel foil, platinum foil, and saturated Calomel electrode were used as working, counter, and reference electrodes. Cyclic voltammetric analyses were implemented within potential limits of 0–0.5 V at different scan rates from 5 to 100 mVs^{-1} . Galvanostatic charge/discharge studies were done at various current density values from 1 to 5 Ag^{-1} . The cyclic stability analyses were conducted with continuous 2000 CV cycles at a high scan rate of 100 mVs^{-1} .

3 Results and Discussion

3.1 Thermogravimetric Analysis

The ZnO-3 material (without calcined) was analyzed using the thermogravimetry to investigate the thermal properties, as shown in Fig. 1. TGA analysis was conducted and regulated from room temperature to $900 \text{ }^\circ\text{C}$. The TGA curve has a total weight loss of about 2.2%, similar to previously reported literature [25, 26]. Three weight loss curves were observed in the present TGA curve till $600 \text{ }^\circ\text{C}$, with no additional weight loss spotted at temperature up to $900 \text{ }^\circ\text{C}$. The weight losses observed were at room temperature to $207 \text{ }^\circ\text{C}$, 207 to $400 \text{ }^\circ\text{C}$, and 400 to $600 \text{ }^\circ\text{C}$, respectively. The first weight loss of 0.6% occurred from room temperature to $207 \text{ }^\circ\text{C}$, due to discharge of moisture, Organic molecules, and volatile surfactant molecule. They are physically absorbed on the outer surface of as-prepared zinc complex material during the synthetic process. The second weight loss of 1.2% from 207 to $400 \text{ }^\circ\text{C}$ is due to the evolution of physisorbed and chemisorbed materials. The third weight loss of 0.4% appeared from 400 to $600 \text{ }^\circ\text{C}$, which could be attributed to the complete decomposition of organic moieties

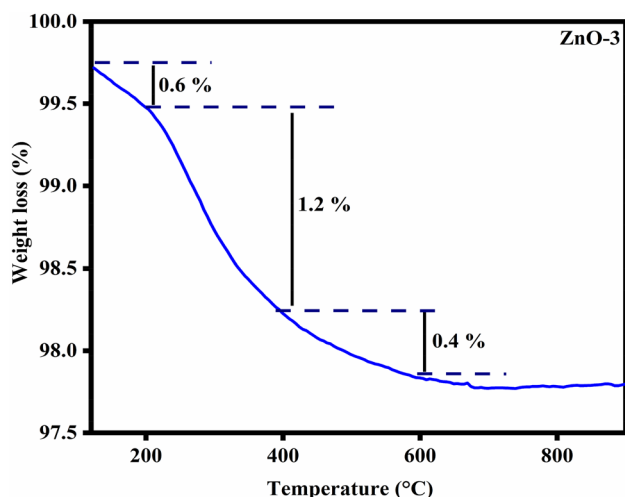


Fig. 1 TGA analysis of ZnO-3 material

and the formation of pure ZnO material. Consequently, the calcination temperature was fixed as 600 °C in this present endeavor.

3.2 X-ray Diffraction Analysis

The crystal structure and phase information of the freshly prepared ZnO samples were obtained by XRD pattern analysis. Figure 2 displays the different XRD patterns of the ZnO materials prepared using three different concentrations of the CTAB template. All the materials were calcined at 600 °C to acquire a pure ZnO crystalline phase. In the entire diffracted patterns, the diffraction peaks appeared at 2θ values of 31.8, 34.5, 36.3, 47.6, 56.7, 63, 66.5, 68.1, 69.2, 72.8

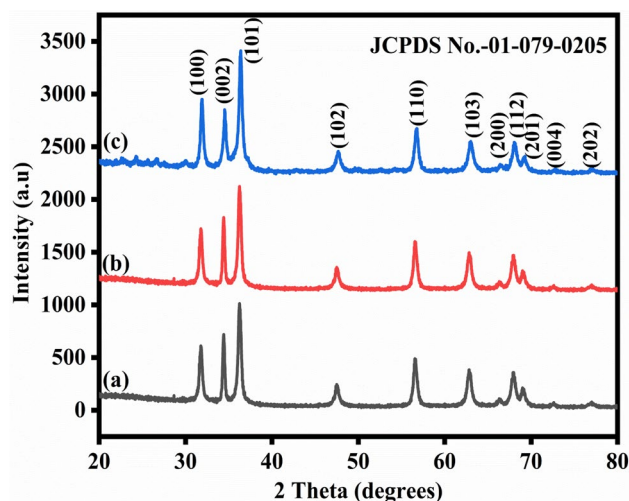


Fig. 2 X-ray diffraction analysis of ZnO materials; (a) ZnO-1, (b) ZnO-2 and (c) ZnO-3 material

and 77.2° which are assigned to (100), (002), (101), (102), (110), (103), (200), (112), (201), (004) and (202) crystallographic planes respectively. All the peaks are well indexed with JCPDS card no.-01-079-0205 demonstrating the development of hexagonal ZnO material with the space group of $P63mc$. There are no extra peaks in the XRD spectrum, which authenticates distinctly pure ZnO material devoid of impurities. All the diffraction patterns provide the same profile except for the variations in their intensities. The XRD analyses confirmed that the present CTAB templated coprecipitation method provides highly pure ZnO material.

3.3 Fourier Transform Infrared Spectroscopy

The different vibrational modes of ZnO materials such as ZnO-1, ZnO-2, and ZnO-3 are characterized by FTIR spectroscopy. Three peaks, evidently visible in the present FTIR spectrums, (Fig. 3) corresponds to ZnO materials' distinctive peaks. Two peaks appeared at 423 and 526 cm^{-1} attributes to the polar stretching vibrational modes of $E1(TO)$ and $E1(LO)$, respectively [27–29]. The peak located at 502 cm^{-1} is described by the vibrational mode of the Zn–O bond. The crystalline and bonding properties of the ZnO materials were confirmed based on the XRD and FTIR characterizations,

3.4 Morphological Analysis

The morphological features of the freshly prepared ZnO-1, ZnO-2, and ZnO-3 materials were explained by employing scanning electron microscopy. Figure 4a and b establishes the low and high magnification SEM images of ZnO-1

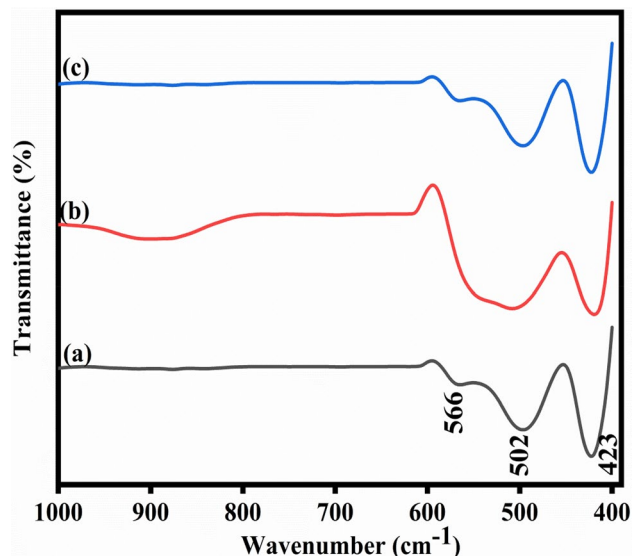
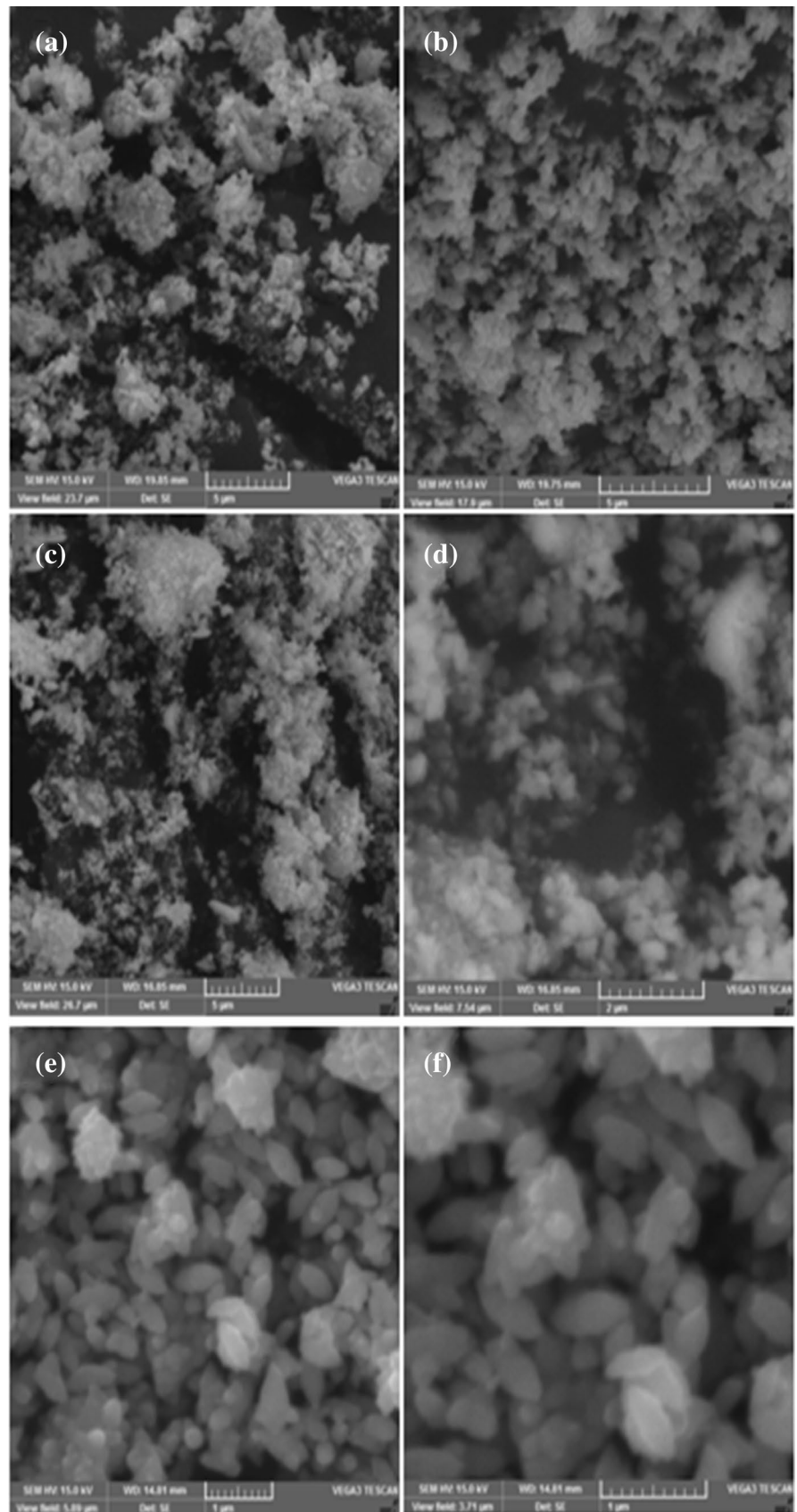


Fig. 3 FTIR spectral analysis of ZnO materials; (a) ZnO-1, (b) ZnO-2 and (c) ZnO-3 material

Fig. 4 Lower and higher magnification SEM images of ZnO materials; **a** and **b** ZnO-1, **c** and **d** ZnO-2 and **e** and **f** ZnO-3 material

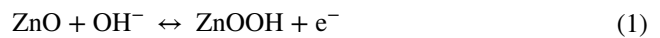


materials, which were prepared without any CTAB template. The lower magnification images of ZnO-1 material exhibits the aggregated like morphologies, whereas the higher magnification images display the minute irregular shaped particles, which confirms that the irregular shaped particles are conjoined and displays an aggregated like morphology. When introducing 1 mM of the CTAB template, ZnO-2 is efficiently generated, describing definite shaped particles displayed in Fig. 4c and d. The lower and higher magnification images of ZnO-3 materials (synthesized using 2 mM of CTAB concentration) were shown in Fig. 4e and f. Notably, the ZnO-3 material exhibited the uniform rice-like morphology. The excellent rice like morphology was created by the CTAB template action, which restricts rice-like ZnO structures' aggregation. The formation mechanism is as follows: The crucial parameters such as counterion properties, charge density, and chemical potentials are the templating process's key factors. The electrostatic property, hydrogen bonding, and vanderwaals force between the entities are also essential factors to assemble principle-oriented nanostructures. Dissolving CTAB in water provides CTA⁺ and Br⁻ entities. However, the zinc nitrate offers a Zn²⁺ ion in water during the dissolving of the precursor. The resultant Zn²⁺ entities joined with the CTAB moieties due to electrostatic attraction forces. During this time, the CTAB alters the morphological properties, which results in the rice-like ZnO structures [23, 30, 31].

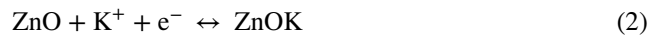
3.5 Electrochemical Supercapacitor Analysis

Elucidation of the rice-like structure's utility in the ZnO structures' electrochemical applications and supercapacitive features was demonstrated by cyclic voltammetry and Galvanostatic charge/discharge analytic techniques. Cyclic voltammetry analyses were conducted to identify the charge storage mechanism, rate capability, and the specific capacitances of the freshly prepared ZnO-1, ZnO-2, and ZnO-3 electrodes, in the potential variation from 0 to 0.5 V at different scan rates such as 5, 10, 25, 50, 75 and 100 mV s⁻¹. For the complete electrochemical characterizations, 1 M KOH was utilized as the electrolyte solution. Figure 5a–c displays the CV curves of ZnO-1, ZnO-2, and ZnO-3 electrodes, respectively. Interestingly, the oxidation peak appears at 0.31 V in CV curves, whereas the reduction peak appears at 0.1 V at a scan rate of 5 mV s⁻¹, which confirms the phenomenon of faradaic redox reaction in ZnO materials. The absence of the electric double layer's ideal rectangular behavior is revealed in all the CV curves. It may lead to the confirmation of the pseudocapacitive charge storage mechanism of ZnO electrode materials [32]. The faradaic process could be either assigned to chemical adsorption/desorption or redox reaction of the functional groups present on the

superficial layer of ZnO electrode materials. Consequently, the faradaic redox reaction is described as follows [33]:



and



When increasing the scan rate from 5 to 100 mV s⁻¹, the anodic peaks migrated from 0.31 to 0.4 V and the cathodic peak drifts from 0.1 to 0.02 V. This establishes the rapid redox and reversible nature of the ZnO electrode materials [34]. The unchanged CV profile and increasing area under the curve with an increase in the scan rate from 5 to 100 mV s⁻¹ are attributed to the electrode materials' good rate capability [35]. The broadening of the potential difference between redox peaks and the increasing redox peak currents is contributed by the freshly prepared ZnO electrodes' rapid electrode polarization capacity. It is conventional that the specific capacitance feature of present electrode materials mainly depends on the area under the CV curves. The ZnO-3 electrode provides a high area under the CV curves than ZnO-1 and ZnO-2 electrodes, and it demonstrates the reason for the superior specific capacitance property of the ZnO-3 electrode. The specific capacitances of the CV curves were calculated using Eq. 3.

$$C_{sp} = \frac{\int idV}{2 \cdot S \cdot \Delta V \cdot m} \quad (3)$$

where $\int idV$ denotes the integral area of the CV curve, ΔV potential window (V), m mass of the active electrode material (mg), and S , the scan rate (mV s⁻¹) from 5 to 100 mVs⁻¹. The specific capacitance values of CV curves are 304, 369, and 457 F g⁻¹ obtained from ZnO-1, ZnO-2, and ZnO-3 electrodes, respectively, at a scan rate of 5 mV s⁻¹. The ZnO-3 electrode display superior specific capacitance at all scan rates when compared with ZnO-1 and ZnO-2 electrodes. The specific capacitance of the ZnO-3 electrode is higher than the previous literatures based on ZnO materials such as ZnO/carbon nanotube (59 F g⁻¹ at 5 mV s⁻¹) [36], graphene-ZnO hybrid nanocomposites (156 F g⁻¹ at 5 mV s⁻¹) [37], ZnO tetrapods (160.4 F g⁻¹ at 1 A g⁻¹) [38], graphene/ZnO nanocomposite (109 F g⁻¹ at 5 mV s⁻¹) [39]. The superior specific capacitance property of the ZnO -3 materials is attributed to its rice-like structure. The edges, corners, and various crystal planes are the key factors for nanoparticles' energy band structure. In the rice-like structure, both the corners expose different edges, whereas the center provides a different structure. These different edges and structures reduce the distance between valence and conduction bands, providing a short pathway for electrons moving during the electrochemical process.

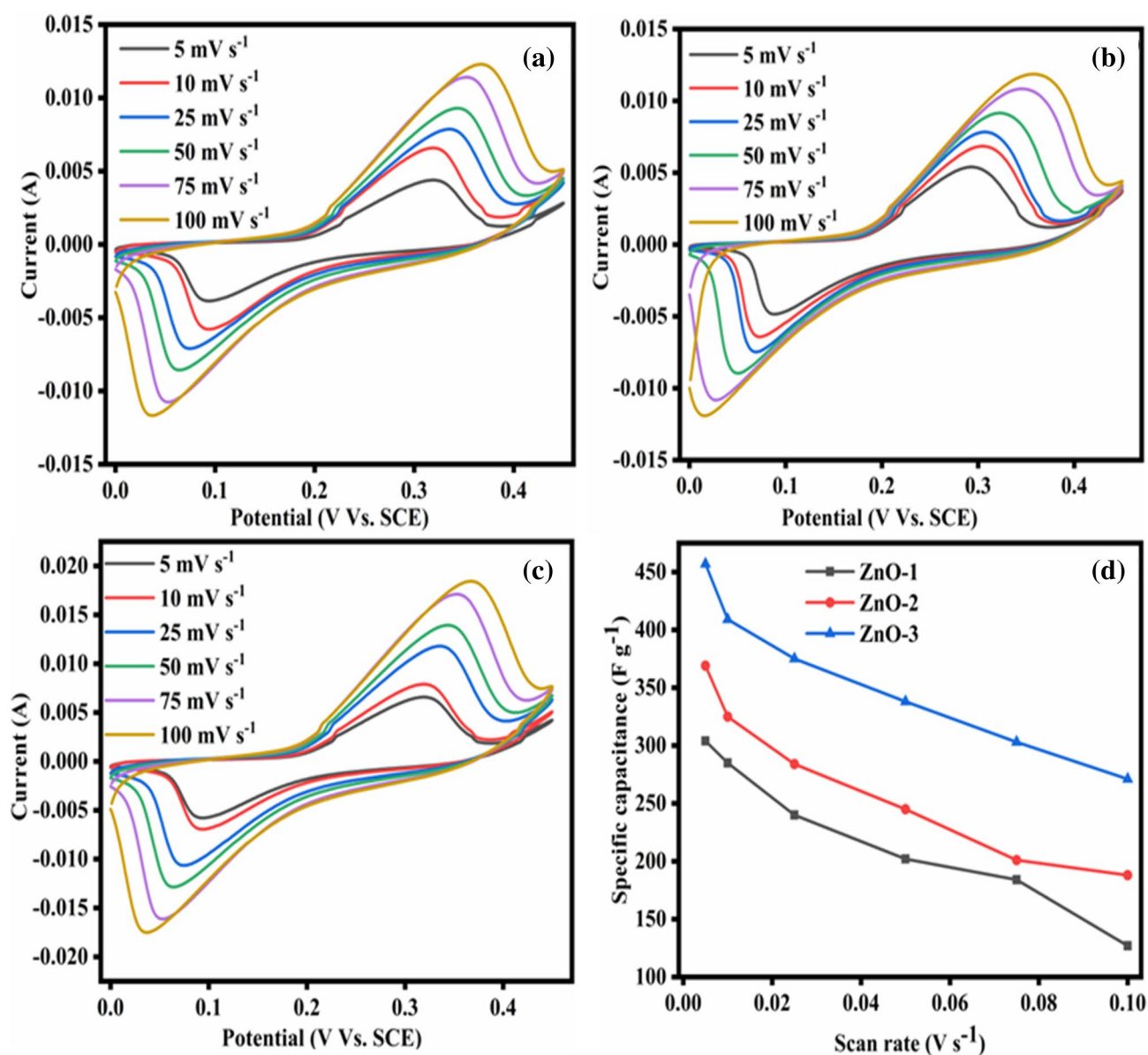


Fig. 5 CV analysis of **a** ZnO-1, **b** ZnO-2 and **c** ZnO-3 materials in 1 M KOH electrolyte; **d** Specific capacitance vs Scan rate

This leads to an increase of specific capacitance in the present endeavor. The calcination temperature such as 600 °C may create more defects in the crystal system, and these defects provide more reaction centers for the electrochemical process, which enhances the super capacitive properties. In the rice-like architecture, the more redox reaction centers actively participated in the redox process, allowing high electrolyte ion utilization [40]. The high utilization of this rice-like structure during electrochemical analysis and redox reaction ultimately leads to high specific capacitance. This redox reaction occurs both in the inner and outer side of the rice like structures that provide higher specific capacitance.

The rate capabilities of the ZnO-1, ZnO-2, and ZnO-3 materials were analyzed through a specific capacitance Vs. Scan rate graph as shown in Fig. 5d. With increasing scan rate, the specific capacitances' calculated values were reduced, which can be due to the following factors: (i) At a high scan rate, the utilization of active materials is significantly smaller due to rapid time, which tends to provide low specific capacitance. (ii) At a low scan rate, the slow scanning allows the utilization of both inner and outer regions of active materials in the electrode and provides higher specific capacitance [41].

In order to efficiently evaluate the specific capacitance and stability properties of the electrode materials, the galvanostatic charge/discharge studies were implemented. The galvanostatic charge/discharge analyses were carried out in the potential window from 0 to 0.45 V at various current densities from 1 to 5 A g⁻¹ as shown in Fig. 6a–c. The non-linear behavior is noticeable in all the GCD curves, and it is varying from a triangular profile that confirms the pseudocapacitive nature. This trend is more consistent with the CV analysis [42]. The GCD curves contain two sections: straight line and curved behavior, which indicates the resistance and capacitance behavior of the ZnO electrode, respectively [32]. The GCD curves of the ZnO-3 electrode possess a long discharge time compared with the other two electrodes, such

as ZnO-1, and ZnO-2 which indicate the superior specific capacitance properties of the ZnO-3 electrode materials. The specific capacitances from GCD curves were calculated using the following Eq. (4)

$$C_{sp} = \frac{I\Delta t}{m\Delta V} \quad (4)$$

where I denotes discharge current density (A), Δt is the discharge time (s), ΔV the potential window (V), and m is the mass of the active material (mg). According to Eq. (4), the ZnO-1, ZnO-2, and ZnO-3 electrodes provide specific capacitances of 275, 342, and 449 Fg⁻¹, respectively, at a current density 1Ag⁻¹. Among all the electrodes, ZnO-3 provides high specific capacitance, and this trend is more

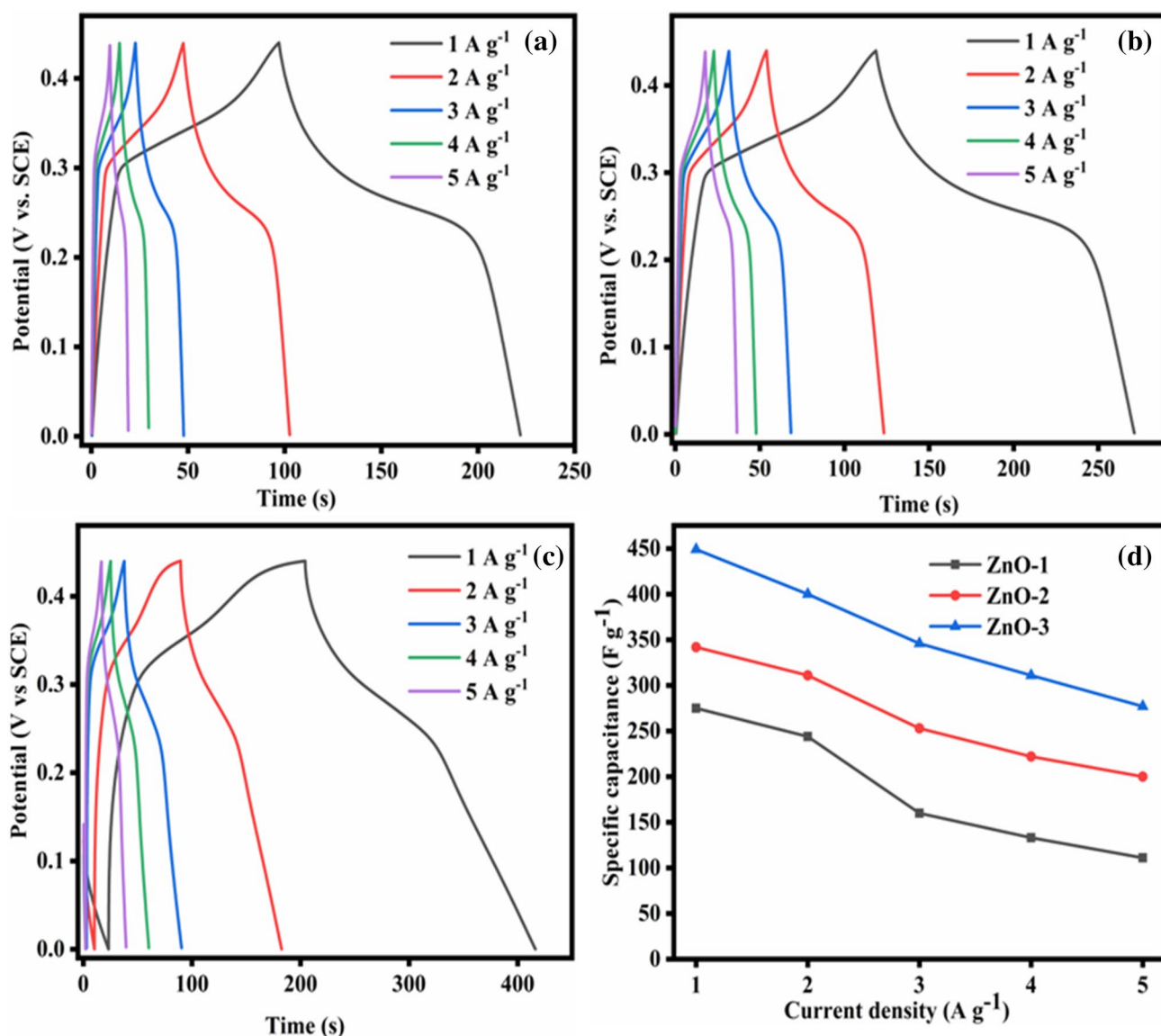


Fig. 6 Galvanostatic charge discharge analysis of **a** ZnO-1, **b** ZnO-2 and **c** ZnO-3 materials in 1 M KOH electrolyte; **d** Specific capacitance vs Scan rate

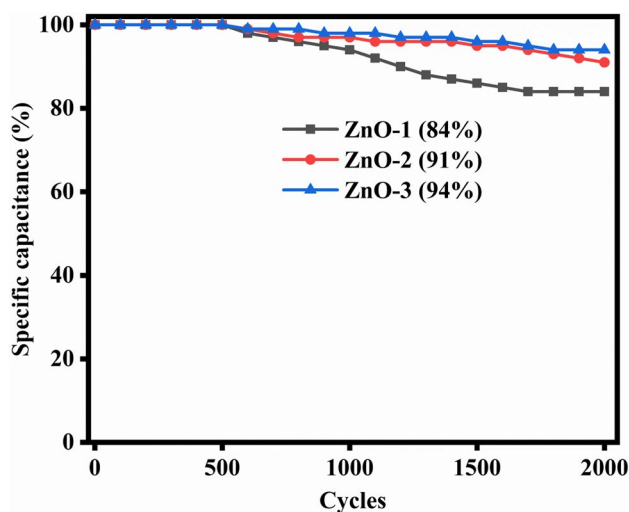


Fig. 7 Cyclic stability analyses of ZnO-1, ZnO-2 and ZnO-3 materials in 1 M KOH electrolyte at 100 mV s^{-1}

consistent with the previously mentioned CV analysis. The specific capacitance Vs the current density graph is shown in 6 d. With the increasing current density, there is a fall in the specific capacitance due to the time limiting process.

Cyclic stability is an essential factor for practical supercapacitor applications. Figure 7 demonstrates the ZnO materials' cyclic stability performance at a scan rate of 100 mV s^{-1} for continuous 2000 cycles. After 2000 continuous CV cycles, the ZnO-1, ZnO-2, and ZnO-3 attain 84, 91, and 94% of the initial specific capacitance, respectively. The ZnO-3 possesses high cyclic stability accredited to the electrodes' large surface area with good accessibility of electrolyte ions to the entire region of rice-like ZnO structures. The obtained superior specific capacitance feature, rate capability, and excellent cyclic stability properties of ZnO-3 electrode are admirable compared with most previous literature, and rice-like ZnO-3 electrode material is one of the most excellent candidates for ultracapacitor application.

4 Conclusion

At this investigation, the rice-like ZnO structure was prepared through a simple and cost-effective CTAB-assisted chemical co-precipitation method followed by a proper calcination process. The thermal properties of the ZnO materials were evaluated employing TGA analysis. The crystalline natures of the materials were demonstrated using XRD analysis, which compliments with JCPDS card no.-01-079-0205 with the hexagonal phase. Furthermore, the FTIR analysis exemplifies the bonding character of the freshly assembled ZnO materials. The SEM analysis explains the prepared ZnO material with 2 mM of CTAB template that exhibits

the uniform rice-like morphology. From electrochemical characterizations, the CV analysis provides a high specific capacitance of 457 Fg^{-1} at a scan rate of 5 mVs^{-1} , whereas GCD curves exhibit the specific capacitance of 449 Fg^{-1} at a current density of 1 Ag^{-1} . The rice-like ZnO-3 materials retained 94% specific capacitance after 2000 continuous CV cycles at a scan rate of 100 mVs^{-1} . These outcomes signify that the rice-like ZnO structure is one of the best suitors as an electrode material for Ultracapacitor applications and energy storage purposes.

References

1. A. Van Dijken, E.A. Meulenlamp, D. Vanmaekelbergh, A. Meijerink, Identification of the transition responsible for the visible emission in ZnO using quantum size effects. *J. Lumin.* **90**, 123–128 (2000). [https://doi.org/10.1016/S0022-2313\(99\)00599-2](https://doi.org/10.1016/S0022-2313(99)00599-2)
2. A.C. Dhanemozhi, V. Rajeswari, S. Sathyajothi, Green synthesis of zinc oxide nanoparticle using green tea leaf extract for supercapacitor application. *Mater. Today Proc.* **4**, 660–667 (2017). <https://doi.org/10.1016/j.matpr.2017.01.070>
3. K. Pradeeswari, A. Venkatesan, P. Pandi, K. Karthik, K.V. Hari Krishna, R. Mohan Kumar, Study on the electrochemical performance of ZnO nanoparticles synthesized via non-aqueous sol-gel route for supercapacitor applications. *Mater. Res. Express* **6**, 105525 (2019). <https://doi.org/10.1088/2053-1591/ab3cae>
4. V. Sahu, S. Goel, R.K. Sharma, G. Singh, Zinc oxide nanoring embedded lacey graphene nanoribbons in symmetric/asymmetric electrochemical capacitive energy storage. *Nanoscale*. **7**, 20642–20651 (2015). <https://doi.org/10.1039/c5nr06083d>
5. K.S. Lee, C.W. Park, J.D. Kim, Electrochemical properties and characterization of various ZnO structures using a precipitation method. *Colloids Surf. A* **512**, 87–92 (2017). <https://doi.org/10.1016/j.colsurfa.2016.10.022>
6. C.B. Ong, L.Y. Ng, A.W. Mohammad, A review of ZnO nanoparticles as solar photocatalysts: synthesis, mechanisms and applications. *Renew. Sustain. Energy Rev.* **81**, 536–551 (2018). <https://doi.org/10.1016/j.rser.2017.08.020>
7. K. Keis, C. Bauer, G. Boschloo, A. Hagfeldt, K. Westermark, H. Rensmo et al., Nanostructured ZnO electrodes for dye-sensitized solar cell applications. *J. Photochem. Photobiol. A* **148**, 57–64 (2002). [https://doi.org/10.1016/S1010-6030\(02\)00039-4](https://doi.org/10.1016/S1010-6030(02)00039-4)
8. D. Barreca, D. Bekermann, E. Comini, A. Devi, R.A. Fischer, A. Gasparotto et al., Urchin-like ZnO nanorod arrays for gas sensing applications. *CrystEngComm* **12**, 3419–3421 (2010). <https://doi.org/10.1039/c0ce00139b>
9. K.C. Barick, S. Nigam, D. Bahadur, Nanoscale assembly of mesoporous ZnO: a potential drug carrier. *J. Mater. Chem.* **20**, 6446–6452 (2010). <https://doi.org/10.1039/c0jm00022a>
10. S.K. Arya, S. Saha, J.E. Ramirez-Vick, V. Gupta, S. Bhansali, S.P. Singh, Recent advances in ZnO nanostructures and thin films for biosensor applications: review. *Anal. Chim. Acta.* **737**, 1–21 (2012). <https://doi.org/10.1016/j.aca.2012.05.048>
11. Z.F. Shi, Y.T. Zhang, X.J. Cui, S.W. Zhuang, B. Wu, J.Y. Jiang et al., Epitaxial growth of vertically aligned ZnO nanowires for bidirectional direct-current driven light-emitting diodes applications. *CrystEngComm* **17**, 40–49 (2015). <https://doi.org/10.1039/c4ce01788a>
12. Y. Qiu, S. Yang, ZnO nanotetrapods: controlled vapor-phase synthesis and application for humidity sensing. *Adv. Funct. Mater.* **17**, 1345–1352 (2007). <https://doi.org/10.1002/adfm.200601128>

13. P. Singh, A. Kumar, A. Kaushal, D. Kaur, A. Pandey, R.N. Goyal, In situ high temperature XRD studies of ZnO nanopowder prepared via cost effective ultrasonic mist chemical vapour deposition. *Bull. Mater. Sci.* **31**, 573–577 (2008). <https://doi.org/10.1007/s12034-008-0089-y>
14. B. Baruwati, D.K. Kumar, S.V. Manorama, Hydrothermal synthesis of highly crystalline ZnO nanoparticles: a competitive sensor for LPG and EtOH. *Sens. Actuators B* **119**, 676–682 (2006). <https://doi.org/10.1016/j.snb.2006.01.028>
15. M. Zare, K. Namratha, K. Byrappa, D.M. Surendra, S. Yallappa, B. Hungund, Surfactant assisted solvothermal synthesis of ZnO nanoparticles and study of their antimicrobial and antioxidant properties. *J. Mater. Sci. Technol.* **34**, 1035–1043 (2018). <https://doi.org/10.1016/j.jmst.2017.09.014>
16. C. He, T. Sasaki, Y. Shimizu, N. Koshizaki, Synthesis of ZnO nanoparticles using nanosecond pulsed laser ablation in aqueous media and their self-assembly towards spindle-like ZnO aggregates. *Appl. Surf. Sci.* **254**, 2196–2202 (2008). <https://doi.org/10.1016/j.apsusc.2007.09.007>
17. F.T. Thema, E. Manikandan, M.S. Dhlamini, M. Maaza, Green synthesis of ZnO nanoparticles via *Agathosma betulina* natural extract. *Mater. Lett.* **161**, 124–127 (2015). <https://doi.org/10.1016/j.matlet.2015.08.052>
18. Y.F. Gao, M. Nagai, Y. Masuda, F. Sato, K. Koumoto, Electrochemical deposition of ZnO film and its photoluminescence properties. *J. Cryst. Growth.* **286**, 445–450 (2006). <https://doi.org/10.1016/j.jcrysgro.2005.10.072>
19. Y. Ma, F. Liang, Y. Liu, X. Zhai, J. Liu, Effect of dispersion on visible light transmittance and resistivity of indium tin oxide nanoparticles prepared by cetyltrimethylammonium bromide-assisted co-precipitation method. *J. Mater. Sci. Mater. Electron.* **30**, 17963–17971 (2019). <https://doi.org/10.1007/s10854-019-02150-x>
20. S.A. Hassanzadeh-Tabrizi, Optimization of the synthesis parameters of high surface area ceria nanopowder prepared by surfactant assisted precipitation method. *Appl. Surf. Sci.* **257**, 10595–10600 (2011). <https://doi.org/10.1016/j.apsusc.2011.07.056>
21. A. Kumar, R.K. Upadhyay, Optical, structural and morphological studies of ZnS nanoparticles synthesized using inorganic capping agent. *J. Mater. Sci.* **26**, 2430–2435 (2015). <https://doi.org/10.1007/s10854-015-2702-3>
22. Y. Wang, A.S. Angelatos, F. Caruso, Template synthesis of nanostructured materials via layer-by-layer assembly. *Chem. Mater.* **20**, 848–858 (2008). <https://doi.org/10.1021/cm7024813>
23. Y.X. Wang, J. Sun, X. Fan, X. Yu, A CTAB-assisted hydrothermal and solvothermal synthesis of ZnO nanopowders. *Ceram. Int.* **37**, 3431–3436 (2011). <https://doi.org/10.1016/j.ceramint.2011.04.134>
24. A. Cai, A. Guo, Y. Chang, Y. Sun, S. Xing, Z. Ma, Fast synthesis of DNA-assisted flower-like ZnO superstructures with improved photocatalytic and antibacterial performances. *Mater. Lett.* **111**, 158–160 (2013). <https://doi.org/10.1016/j.matlet.2013.08.085>
25. O. Arslan, A.P. Singh, Cysteine-functionalized zwitterionic ZnO quantum dots. *J. Mater. Res.* **28**, 1947–1955 (2013)
26. L.A.A. Chunduri, A. Kurdekar, B.E. Pradeep, M.K. Haleygirisetty, K. Venkataramaniah, I.K. Hewlett, Streptavidin conjugated ZnO nanoparticles for early detection of HIV infection. *Adv. Mater. Lett.* **8**, 472–480 (2017)
27. M. Sundrarajan, S. Ambika, K. Bharathi, Plant-extract mediated synthesis of ZnO nanoparticles using *Pongamia pinnata* and their activity against pathogenic bacteria. *Adv. Powder Technol.* **26**, 1294–1299 (2015). <https://doi.org/10.1016/j.apt.2015.07.001>
28. A. Sahai, N. Goswami, Structural and vibrational properties of ZnO nanoparticles synthesized by the chemical precipitation method. *Phys. E* **58**, 130–137 (2014). <https://doi.org/10.1016/j.physe.2013.12.009>
29. N. Goswami, D.K. Sharma, Structural and optical properties of unannealed and annealed ZnO nanoparticles prepared by a chemical precipitation technique. *Phys. E* **42**, 1675–1682 (2010). <https://doi.org/10.1016/j.physe.2010.01.023>
30. R.K. Shukla, K.K. Raina, Soft templated zinc oxide nanostructures and their colloidal assemblies for optical, capacitive and ionic impurity capturing applications. *Solid State Sci.* **104**, 106201 (2020). <https://doi.org/10.1016/j.solidstatesciences.2020.106201>
31. R.K. Shukla, P. Chamoli, K.K. Raina, Lyotropic liquid crystalline nano templates for synthesis of ZnS cogwheels. *J. Mol. Liq.* **283**, 667–673 (2019). <https://doi.org/10.1016/j.molliq.2019.03.139>
32. J. Yesuraj, S.A. Suthanthiraraj, O. Padmaraj, Materials science in semiconductor processing synthesis, characterization and electrochemical performance of DNA-templated Bi₂MoO₆ nanoplates for supercapacitor applications. *Mater. Sci. Semicond. Process.* **90**, 225–235 (2019). <https://doi.org/10.1016/j.mssp.2018.10.030>
33. F. Naeem, S. Naeem, Z. Zhao, G. Qiang Shu, J. Zhang, Y. Mei et al., Atomic layer deposition synthesized ZnO nanomembranes: a facile route towards stable supercapacitor electrode for high capacitance. *J. Power Sources.* **451**, 227740 (2020). <https://doi.org/10.1016/j.jpowsour.2020.227740>
34. D. He, G. Liu, A. Pang, Y. Jiang, H. Suo, C. Zhao, A high-performance supercapacitor electrode based on tremella-like NiCo₂O₄@NiO core/shell hierarchical nanostructures on nickel foam. *Dalt. Trans.* **46**, 1857–1863 (2017). <https://doi.org/10.1039/c6dt04500f>
35. F. Paquin, J. Rivnay, A. Salleo, N. Stingelin, C. Silva, Multi-phase semicrystalline microstructures drive exciton dissociation in neat plastic semiconductors. *J. Mater. Chem. C.* **3**, 10715–10722 (2015). <https://doi.org/10.1039/b000000x>
36. L.S. Aravinda, K.K. Nagaraja, H.S. Nagaraja, K.U. Bhat, B.R. Bhat, ZnO/carbon nanotube nanocomposite for high energy density supercapacitors. *Electrochim. Acta.* **95**, 119–124 (2013). <https://doi.org/10.1016/j.electacta.2013.02.027>
37. Z. Li, Z. Zhou, G. Yun, K. Shi, X. Lv, B. Yang, High-performance solid-state supercapacitors based on graphene-ZnO hybrid nanocomposites. *Nanoscale Res. Lett.* **8**, 1–9 (2013). <https://doi.org/10.1186/1556-276X-8-473>
38. Q. Luo, P. Xu, Y. Qiu, Z. Cheng, X. Chang, H. Fan, Synthesis of ZnO tetrapods for high-performance supercapacitor applications. *Mater. Lett.* **198**, 192–195 (2017). <https://doi.org/10.1016/j.matlet.2017.04.032>
39. A. Ramadoss, S.J. Kim, Facile preparation and electrochemical characterization of graphene/ZnO nanocomposite for supercapacitor applications. *Mater. Chem. Phys.* **140**, 405–411 (2013). <https://doi.org/10.1016/j.matchemphys.2013.03.057>
40. R. Zou, K. Xu, T. Wang, G. He, Q. Liu, X. Liu, Z. Zhang, J. Hu, Chain-like NiCo₂O₄ nanowires with different exposed reactive planes for high-performance supercapacitors. *J. Mater. Chem. A.* **1**, 8560–8566 (2013). <https://doi.org/10.1039/c3ta11361b>
41. T. Liu, H. Chai, D. Jia, Y. Su, T. Wang, W. Zhou, Rapid microwave-assisted synthesis of mesoporous NiMoO₄ nanorod/reduced graphene oxide composites for high-performance supercapacitors. *Electrochim. Acta.* **180**, 998–1006 (2015). <https://doi.org/10.1016/j.electacta.2015.07.175>
42. J. Yesuraj, S.A. Suthanthiraraj, Bio-molecule templated hydrothermal synthesis of ZnWO₄ nanomaterial for high-performance supercapacitor electrode application. *J. Mol. Struct.* **1181**, 131–141 (2019). <https://doi.org/10.1016/j.molstruc.2018.12.087>

Publisher's Note Springer Nature remains neutral with regard to jurisdictional claims in published maps and institutional affiliations.

Authors and Affiliations

Kunhikrishnan Lakshmi^{1,2} · Shanmugham Revathi¹

✉ Shanmugham Revathi
sreva_2003@yahoo.co.in

² Department of Chemistry, Anand Institute of Higher
Technology, OMR Road, Chennai 603103, India

¹ Department of Chemistry, College of Engineering, Anna
University, Guindy Campus, Chennai 600025, India